PHILOSOPHICAL TRANSACTIONS A

rsta.royalsocietypublishing.org

Review

Cite this article: Natarajan B, Gilman JW. 2018 Bioinspired Bouligand cellulose nanocrystal composites: a review of mechanical properties. *Phil. Trans. R. Soc. A* **376**: 20170050.
http://dx.doi.org/10.1098/rsta.2017.0050

Accepted: 9 August 2017

One contribution of 14 to a discussion meeting issue 'New horizons for cellulose nanotechnology'.

Subject Areas:
materials science, nanotechnology

Keywords:
cellulose nanocrystals, Bouligand, extrinsic toughening, self-assembly, chiral nematic, nanocomposites

Author for correspondence:
Jeffrey W. Gilman
e-mail: jwgilman@nist.gov

THE ROYAL SOCIETY PUBLISHING

Bioinspired Bouligand cellulose nanocrystal composites: a review of mechanical properties

Bharath Natarajan[1,2] and Jeffrey W. Gilman[1]

[1]Material Measurement Laboratory, National Institute of Standards and Technology, Gaithersburg, MD 20899, USA
[2]Department of Physics, Georgetown University, Washington, DC 20057, USA

JWG, 0000-0003-4441-8698

The twisted plywood, or Bouligand, structure is the most commonly observed microstructural motif in natural materials that possess high mechanical strength and toughness, such as that found in bone and the mantis shrimp dactyl club. These materials are isotropically toughened by a low volume fraction of soft, energy-dissipating polymer and by the Bouligand structure itself, through shear wave filtering and crack twisting, deflection and arrest. Cellulose nanocrystals (CNCs) are excellent candidates for the bottom-up fabrication of these structures, as they naturally self-assemble into 'chiral nematic' films when cast from solutions and possess outstanding mechanical properties. In this article, we present a review of the fabrication techniques and the corresponding mechanical properties of Bouligand biomimetic CNC nanocomposites, while drawing comparison to the performance standards set by tough natural composite materials.

This article is part of a discussion meeting issue 'New horizons for cellulose nanotechnology'.

1. Introduction

Biological composites are efficient, multi-functional materials that achieve optimum performance through complex structural hierarchy and a relatively sparse choice of chemical constituents [1–3]. These composites exhibit a combination of superior toughness, modulus, fatigue tolerance, responsiveness to strain rate, resistance

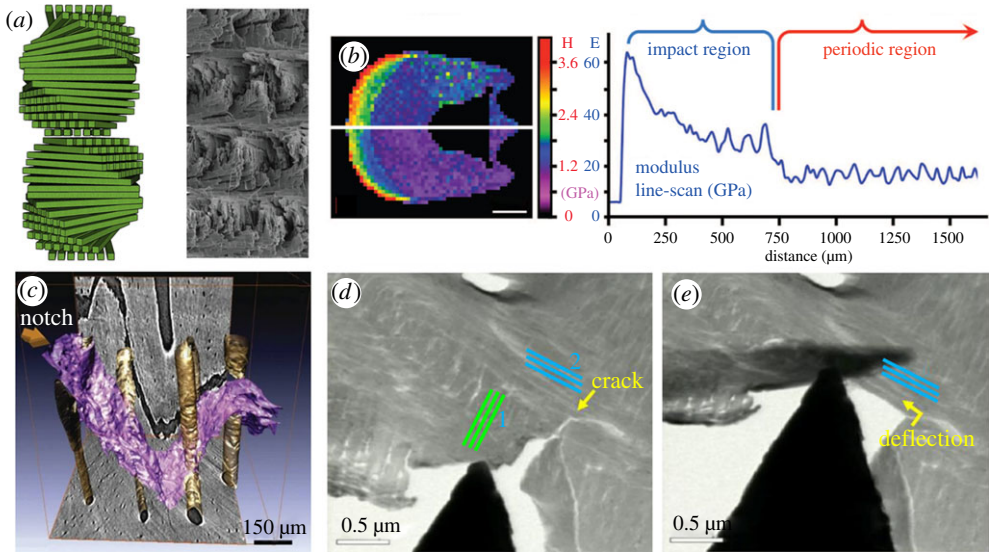

Figure 1. (*a*) Comparison of a 3D model Bouligand structure with SEM image of chitin fibril arrangement in the mantis shrimp dactyl club. (*b*) Nanoindentation map of hardness and a line profile of elastic modulus from the impact region to the periodic region. Reproduced with permission [7]. Copyright © 2012, AAAS. (*c*) 3D X-ray computed microtomograph of crack paths (purple) in human cortical bone, showing crack twisting and deflection around Haversian canal network (yellow). Reproduced with permission [8]. Copyright © 2012, Elsevier. (*d*,*e*) *In situ* TEM micrographs of picoindentation performed on focused ion beam milled dactyl club impact region, showing 90° crack deflection at interface between perpendicular fibre bundles (green and blue). Reproduced with permission [9]. Copyright © 2016, Wiley.

to impact and extreme environments, self-healing behaviour as well as secondary properties such as iridescence for signalling [1–4]. Characteristically, they are composed of a majority fraction of hard, mineralized particles in periodic arrangement with long-range ordered organic phase. While in nacre or abalone shell, this ordering is observed to resemble 'brick and mortar' stacking [5], in most other organisms, the evolutionarily convergent solution to toughness is observed to be the Bouligand (or twisted plywood/helicoidal/chiral nematic/cholesteric) arrangement. Indeed, this is the most commonly observed motif in extracellular composite architecture [6]. Here, the constituent fibrils are arranged in layers stacked in a helical fashion, i.e. the fibrils are parallel within each layer but their direction rotates by a fixed angle between layers (figure 1*a*) [10].

Bouligand composites, such as crustacean shells [11], ivory [12] and bone [13], have the unique quality of being tough without being ductile. The superior toughness of these composites results from structural toughening, taking place at fixed length scales, due to the hierarchical and periodic arrangement of the hard and soft phases [14]. The Bouligand architecture is observed to maximize energy dissipation through crack bridging, deflection, arrest and twisting [9]. While crack deflection and arrest slow down crack propagation, crack twisting allows multiple cracks to grow from various nucleation sites without coalescing. This high crack surface to volume ratio maximizes energy dissipation. Crack bridging at impact locations provides additional toughening by minimizing crack-tip stress concentration and arresting further crack opening. Using these strategies and a minimal inventory of materials (chitin, collagen, cellulose, proteins, calcium phosphate and calcium carbonate), Nature has built tough materials with wide-ranging properties (≈1–70 GPa in modulus and 20–300 MPa tensile strength) and functionalities.

The excellent characteristics of natural composites have inspired many works of biomimicry using synthetic building blocks [2,15]. Researchers have successfully fabricated 'brick and mortar'

architectures using layered materials such as clay and graphene, with properties akin to or exceeding those of nacre [2]. However, the Bouligand architecture has thus far received less attention. This is probably due to the additional complexity involved in creating a helical twist to the layer-by-layer stacking [16]. However, cellulose nanocrystals (CNCs) are chiral rod-like particles that readily self-assemble into Bouligand structures with periodicities in the visible wavelength range [17]. This behaviour is similar to that observed in other chiral rod-like species such as collagen, chitin, tobacco mosaic virus and DNA. CNCs are isolated by the acid hydrolysis of sustainable cellulosic sources such as wood, bacteria and tunicates, and vary greatly in size, shape and crystalline content based on the source material [18–21]. Owing to the large fraction of highly ordered cellulose chains, CNCs exhibit remarkable elastic moduli (≈143 GPa), but at low polymer-like densities (≈1.62 g cm^{-3}) [22,23]. These characteristics identify CNCs as excellent candidate building blocks for Bouligand nanocomposites. However, an overwhelming majority of the work on the self-assembled CNC materials has been focused on understanding the assembly process and its effect on photonic properties [17]. While several means to fabricate CNC Bouligand nanocomposites have been proposed (template filling [24], one-step casting [25,26], *in situ* polymerization [27]), only a handful of articles report their mechanical properties.

In this article, we present a review of the fabrication techniques and the corresponding mechanical properties of Bouligand CNC nanocomposites. Firstly, we summarize the literature on biological Bouligand composites, highlighting their pervasiveness in Nature and the breadth of material properties exhibited. Then, we discuss the unique advantages offered by the Bouligand structure and review learnings from top-down fabricated Bouligand fibre-reinforced composites. Following this section, a brief summary of CNC self-assembly is provided, with emphasis on the key parameters affecting the assembly process. We then present the various techniques employed to fabricate CNC Bouligand composites, their merits and limitations. Further, we determine the applicability of these techniques for bio-emulation by comparing the mechanical properties of synthetic and natural Bouligand composites. We then identify the limitations of the polymer nanocomposite (PNC) approach in mimicking the mechanical performance of touchstone biological materials. Pristine CNC films with enhanced stiffness and strain to failure are deemed necessary for the effectiveness of the PNC approach. We conclude by suggesting alternative strategies for concurrently improving the pristine film properties such as stiffness and strain to failure. With this review, we hope to motivate future research on this topic.

2. Natural Bouligand composites

Yves Bouligand, from whom the Bouligand arrangement derives its name[1], was the first to identify this microstructural motif and its similarity to the (then) emergent liquid crystalline material class in the 1960s [10,32–36]. Bouligand is also credited for working towards proving that a small number of fundamental structural motifs are at the origin of all the various forms seen in Nature. As if to confirm his hypothesis, with every passing year, more tough biological materials are being discovered to possess an underlying Bouligand structure. Crustacean exoskeletons (crab and lobster shells) were the earliest natural materials to be found to have a twisted plywood arrangement [10]. The fundamental units in these structures are 50–300 nm diameter composite fibres comprising aligned 3 nm chitin fibrils wrapped in proteins. The fibres are stacked in a helical fashion, with a decreasing gradient in pitch away from the shell surface, leading to graded mechanical properties [11,37]. Although the fundamental building blocks are identical across the crustaceans, the mechanical properties have been found to vary significantly from organism to organism. Some crab shells are relatively weak and brittle. The dry state modulus, tensile

[1]We note that some studies prefer to use the terms 'helicoidal' or 'twisted plywood' to denote this arrangement and use 'Bouligand' to refer only to the wavy pattern observed in oblique sections (see image in §3) of these materials. However, several others refer to the helically stacked structure itself as the Bouligand structure [9,28–31]. We use the terms 'helicoidal', 'twisted plywood' and 'Bouligand' interchangeably here.

strength and strain to failure of sheep crab shells were found to be 764 ± 83 MPa, 12.9 ± 1.7 MPa and $1.8 \pm 0.3\%$, respectively [37]. The American lobster cuticle, on the other hand, is found to be significantly tougher, with the modulus varying from 8 GPa to 4 GPa from the surface to the bulk, and tensile strengths of 100–150 MPa [38,39]. However, the hardness of the lobster cuticle is found to be lower due to lower surface mineral content in the form of crystalline calcium carbonate (948 MPa > 270 MPa of the lobster) [38]. Another important design feature of crustacean shells is the network of helicoidal pore canals embedded in the Bouligand structure. The pore canals, made of chitin, serve to transport ions that replenish the mineral phase after moulting. Additionally, the canals result in the arrangement of the helicoidally stacked fibres into a higher-length-scale honeycomb-like structure. This ordering leads to increased structural anisotropy, out-of-plane stiffness and fracture resistance [28].

Mammalian bones and antlers are thematically similar materials with distinct differences dictated by function [38]. Both materials are observed to contain a 'cancellous' region surrounded by compact bone, which is constituted of osteons (10–500 µm in diameter). The osteons comprise concentric layers of parallel 0.5 µm collagen fibrils with dispersed hydroxyapatite nanocrystals. These layers are arranged in a twisted plywood pattern with the helical director pointing perpendicular to the osteon axis [13]. The mechanical properties of compact bone, which have been widely reported in the literature, are excellent, with elastic moduli and tensile strengths of 15–20 GPa and 100–160 MPa, respectively. Antlers are measured to be less stiff, but similar in strength. The highest moduli (11.6 GPa) and tensile strengths (≈300 MPa) measured are those of the North American moose (*Alces alces*) [40].

Ivory, a material renowned for its strength and toughness, is found in the tusks of elephant, hippopotamus, walrus, warthog and whales [12]. Barring subtle variations from animal to animal, it generally comprises an organic framework of collagen fibril (1 µm diameter) layers, arranged in a twisted plywood pattern, binding an inorganic matrix of hydroxyapatite particles. The collagen fibrils themselves comprise 300 nm long, 1.2 nm wide collagen molecules with hydroxyapatite platelets filling end-to-end gaps [12,41]. On average, the measured modulus and tensile strength of these materials are comparable to those of bone and antlers (10 GPa and ≈100 MPa, respectively) [41]. In addition to being tough and resilient, ivory variants such as the narwhal tusk, rich in nerves, are also hypothesized to provide environmental sensing abilities [42].

The most remarkable showcase of the mechanical superiority offered by the Bouligand arrangement is the dactyl club of the mantis shrimp (*Odontodactylus scyllarus*) [7]. Mantis shrimps are stomatopods that employ their hammer-like appendages to break open the toughened shells of organisms such as clams and crabs. These appendages are exceptionally damage-tolerant. During the hammering process, they reach accelerations greater than $10\,000g$ and endure large impact forces (1500 N) and high local stresses caused by the collapsing of cavitation bubbles [7]. Additionally, they are able to maintain their structural integrity over thousands of cycles of intense loading, before being replaced during moulting. Through nanoindentation and energy-dispersive X-ray spectroscopy measurements, Weaver *et al.* found that the dactyl club exhibited hierarchical arrangement with regions of graded material properties that provide impact resistance at the surface as well as toughening in the bulk (figure 1*a*,*b*) [7]. The bulk of the club was found to be periodic, comprising crystalline chitin fibrils arranged in a pitch-graded Bouligand arrangement with amorphous calcium carbonate and calcium phosphate [7]. While this region was measured to be of lower hardness and modulus (20–25 GPa), it was found to provide excellent energy dissipation through the chitin fibrils and toughening through crack twisting and deflection in the Bouligand structure. The outermost layer, i.e. the impact region, exhibited the highest hardness and a large modulus of nearly 70 GPa due to the large concentration of highly oriented, crystalline hydroxyapatite ($Ca_5(PO_4)_3(OH)$) [7]. Here, too, the chitin fibres were found to be helicoidally arranged normal to the club surface. Recent studies have revealed an intermediate level of hierarchy where the helicoidal fibres are compacted laterally into a sinusoidal herringbone pattern, thereby enabling additional toughening mechanisms [9].

Meyers' group identified the scales of the Amazonian arapaima fish to possess a similar Bouligand-type structure constituted of helicoidally stacked collagen fibres mineralized by

hydroxyapatite crystals, which provide resistance to piranha bites [43]. Owing to a lower mineral content, the tensile modulus and strength were found to be quite low (1.2 GPa and 47 MPa, respectively). However, the indentation modulus, which is more representative of bite resistance, was observed to be as high as 30–40 GPa [44]. A similar Bouligand motif, of entirely polymeric composition and with lower helical modulation length scales (in the visible wavelength range), was observed to provide wear resistance and fatigue life in some beetle exoskeletons [45]. Natural composites that comprise helicoidally stacked cellulose are observed in plant cell walls, tunicates and tough iridescent fruit shells [6,46,47]. Other instances of the Bouligand arrangement in Nature include some egg shells, deep sea worms, brown seaweeds, algae, ferns, coniferous trees, several other arthropod exoskeletons, cysts of sponges, jellyfish, eelworms, corneal tissues of amphibians, chicken, turtle carapace, etc. [6]. Evidently, the Bouligand structure is the most common motif in extracellular fibrous architecture.

While the role of the specific structure and composition in affecting the observed diversity in properties is not well understood, several underlying mechanisms have been proposed to explain the remarkable strength and toughness of the Bouligand structure. The strength is believed to arise from the hard mineral phase and the ability of the soft protein binder to absorb energy at small length scales [1,14]. This material plasticity enables inelastic, irreversible deformation such as local fibrillar shearing and viscoplasticity, which aids in retarding crack initiation and growth in an isotropic fashion [30]. The toughness is attributed to the ability of the hierarchical Bouligand structure to slow down crack propagation by crack twisting, arrest, deflection or bridging at a fixed length scale [1,3,9,14]. Yaraghi *et al.* [9] presented a clear demonstration of crack deflection at the interface between helicoidal layers in a dactyl club, through *in situ* transmission electron microscopy (TEM) picoindentation (figure 1). Further through nanoindentation these authors demonstrated that the cracks emanating from the indent were arrested at interfaces between in-plane and out-of-plane fibres. Recent studies have also found the Bouligand structure to exhibit phononic bandgaps arising from the spatial periodicity that cause shear wave filtering, i.e. absorption at specific energy levels, leading to enhanced impact tolerance [29]. Remarkably, these materials are also found to respond to increased strain rates with increased energy-absorbing capacity.

These toughening mechanisms, which have also been observed in the other natural composites discussed above, have motivated research endeavours to design and fabricate helicoidally arranged fibre-reinforced composites [48–51]. Chen *et al.* [49] observed the twisted plywood composites to have significantly higher fracture toughness as compared to unidirectional materials. Apichattrabrut & Ravi-Chandar found that helicoidal stacking offered improved debonding resistance and damage tolerance [51]. In agreement with Chen *et al.*, they too measured improved energy absorption and demonstrated high penetration resistance in impact tests in comparison to traditional quasi-isotropic aerospace designs. Similar results for carbon fibre–epoxy composites were described by Grunenfelder *et al.* [50], who also demonstrated through finite-element models that smaller offsets in orientation between layers resulted in a wider spread of damage (figure 2). Yang *et al.* [16] fabricated Bouligand nanocomposites of carbon nanotubes in a photocurable resin using an electrically assisted three-dimensional (3D) printing process. Here, helicoidal stacking was achieved by aligning the nanotubes in each layer (25 µm) to an external electric field, while rotating the field direction from layer to layer. These materials were found to be mechanically superior to composites with randomly dispersed nanotubes. Similar to the carbon fibre composites, a smaller twist angle was found to yield enhanced toughness [16].

While such top-down methods (carbon fibre lay-up, 3D printing) have been employed to understand the advantages offered by the helicoidal stacking [9,50], there have been few successful attempts at replicating the Bouligand structure using nano-sized components [16]. This is attributable to the additional level of complexity involved in adding a periodic twist to the layer-by-layer stacking. In the next section, we offer a brief review of CNCs, which naturally self-assemble in the Bouligand arrangement, thereby presenting a solution to nano-reinforced Bouligand composites.

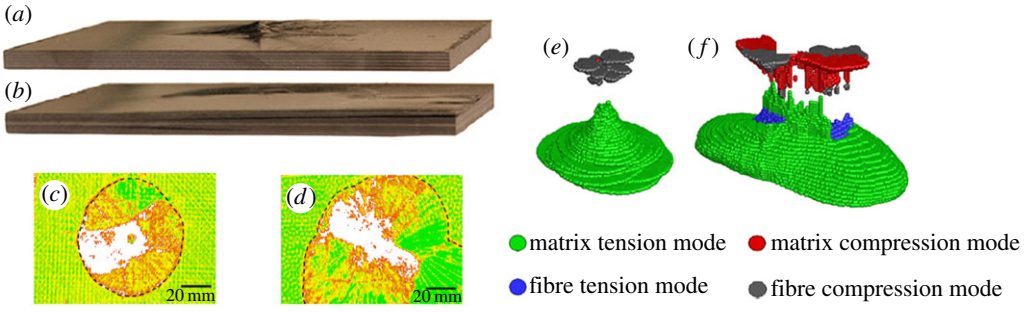

Figure 2. Photographs showing damage in (*a*) quasi-isotropic and (*b*) small-angle Bouligand carbon fibre-reinforced epoxy composites. Ultrasound images showing damage fields (indicated by dotted lines) in (*c*) quasi-isotropic and (*d*) small-angle Bouligand carbon fibre-reinforced epoxy composites. A visualization of impact damage in finite-element models of (*e*) quasi-isotropic and (*f*) small-angle Bouligand CFRPs, with nodal points coloured based on dominant failure mode. The top layer represents the impact surface. The wider distribution of damage in the Bouligand composites is clear in both the experimental (*d*) and simulation (*f*) results. Reproduced with permission [50]. Copyright © 2014, Elsevier.

3. Cellulose nanocrystal self-assembly

CNCs are anisotropic particles that are isolated from sustainable sources such as wood, bacteria and tunicates through preferential acid hydrolysis of amorphous domains [18,21]. Based on the source material, CNCs vary in length from 100 to 2000 nm, and in cross-sectional width from 6 to 20 nm. Wood CNCs, which are the most widely available and studied CNCs, have square cross-sections of size $\approx 6 \times 6$ nm and aspect ratios around 20 [19]. Owing to their prominence in the currently reviewed literature, the term CNCs in this review will henceforth signify wood–CNCs. In these particles, cellulose chains are tightly packed into monoclinic/triclinic lattices stabilized by inter- and intra-chain van der Waals and hydrogen bonding. Owing to this structure, CNCs display an extraordinary combination of specific stiffness ($\approx$100 MN m kg^{-1}) and strength ($\approx$1800 kN m kg^{-1}). Further, they are biocompatible, non-toxic, sustainably sourced and compliant to surface modification. In addition to these excellent traits, CNCs are also found to readily self-assemble into Bouligand structures with periodicities in the optical wavelength range [17]. These characteristics identify CNCs as highly suited candidates for the fabrication of nano-reinforced synthetic Bouligand composites.

The ability of CNCs to form stable chiral nematic liquid crystalline phases in solution was first discovered by Gray and co-workers [52]. Upon drying these solutions, iridescent films, with photonic bandgaps in the visible wavelength range, were observed to form [17]. The 'chiral nematic' ordering, preserved in the solid material through vitrification, was found to be left-handed and Bragg-reflected left-circularly polarized light at wavelengths corresponding to the periodicity or pitch (distance between layers rotated by 360°) of the helical structure. (We note that these films are not truly liquid crystalline, as they are vitrified away from equilibrium.) These unique optical properties motivated numerous efforts to understand the self-assembly behaviour and controlling factors, for applications ranging from iridescent coatings to optical encryption [53]. Firstly, the self-assembly behaviour was attributed to the inherent, screw-like twisting of the CNCs along their length, due to the transfer of chirality from the molecular cellulose [9,14]. Molecular dynamics simulations revealed that the model cellulose fibrils, when energy-minimized, spontaneously developed a right-handed twist. The magnitude of twist was found to depend on the fibril length and the cross-sectional area [54,55]. Experimental evidence of the right-handed twist was shown by Mezzenga *et al.* [56] through detailed atomic force microscopy and TEM imaging.

The pitch and pitch uniformity have been observed to depend on a wide array of parameters. In our opinion, one of the most important factors is the rate of evaporation of water [57]. By

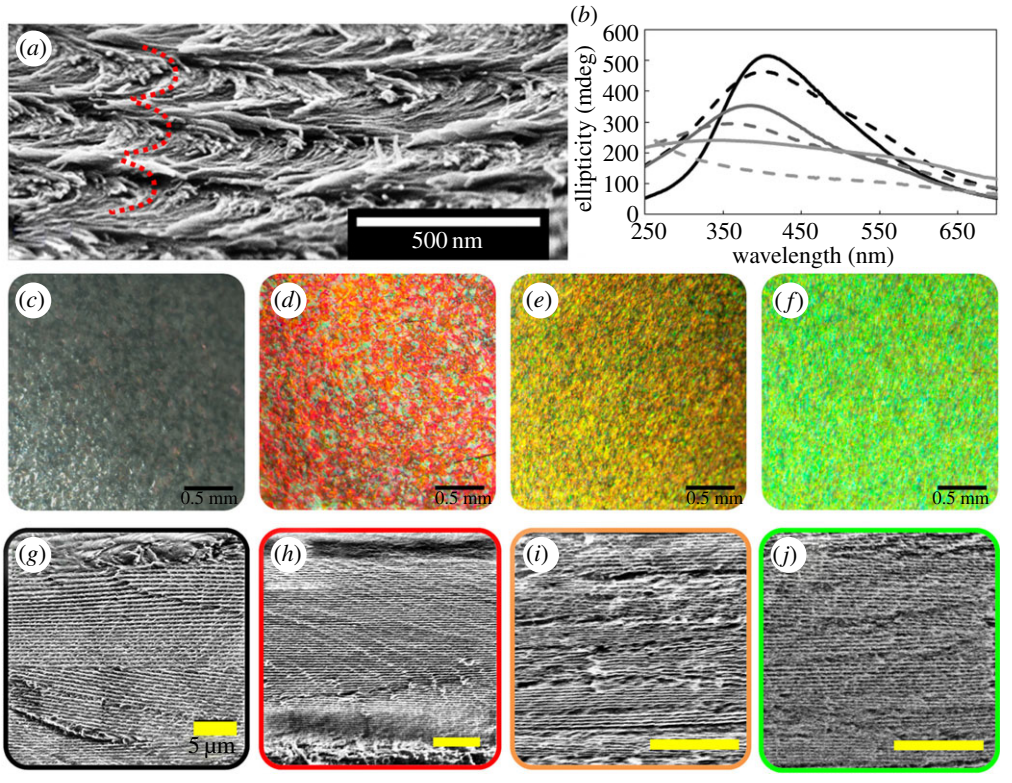

Figure 3. (*a*) An SEM image of a photonic CNC film cross-section showing curves arising from CNC Bouligand arrangement. Reproduced with permission [57]. Copyright © 2017 ACS, Elsevier. (*b*) CD spectra of cellulose films produced from 1% by mass CNC suspensions with 0 (black solid), 0.1 (black dashed), 0.2 (dark grey solid), 0.3 (dark grey dashed), 0.4 (grey solid) and 0.5 mol cm^{-3} (grey dashed) NaCl, showing blue-shifting with increasing ionic strength. Reproduced with permission [58]. Copyright © 2010 ACS, Elsevier. Polarized optical microscopy and SEM images of (*c*,*g*) fast-dried, sodium-neutralized, (*d*,*h*) slow-dried, sodium-neutralized, (*e*,*i*) fast-dried, methyltriphenylphosphonium-neutralized, and (*f*,*j*) slow-dried, methyltriphenylphosphonium-neutralized CNC films. The measured pitch and standard deviations are observed to shift to lower values with slower drying (1000 ± 350 to 606 ± 151 nm) and greater surface hydrophobicity [1000 ± 350 to 619 ± 190 nm (fast) and 606 ± 151 to 504 ± 180 nm (slow)]. Reproduced with permission [57]. Copyright © 2017 ACS, Elsevier.

carefully controlling the drying over the entire casting process, we have revealed that pitch and pitch uniformity bear an inverse relationship to the evaporation rate. In other words, faster evaporation leads to a larger pitch and greater disorder in film structure (figure 3). As the temperature, casting area, air velocity and humidity determine the drying rate, the ability to monitor and control these parameters is essential [59,60]. As the requirement for slow drying limits the scalability of film fabrication, other means to obtain uniform films at reasonable time scales are required. The dependence of the pitch on surface interactions presents a vital avenue. By the addition of varying quantities of electrolyte, the pitch was found to depend inversely on the ionic strength of the solution [21]. Further, we have revealed recently that films of equivalent pitch and uniformity may be obtained at fast drying rates by tuning the surface energy from hydrophilic to hydrophobic [57]. In both these scenarios, the pitch is noted to decrease due to improved chiral interactions between CNCs enabled by the decrease in the electrical double-layer thickness. The pitch and uniformity are also observed to depend on the concentration of the starting solutions. Higher concentrations are found to yield larger pitch and greater sample uniformity. The uniformity of films may also be controlled using shear, electric and magnetic fields: moderate shear, electric and magnetic fields have been found to result in a uniform helical director orientation [58,61,62].

Despite the discovery of CNC self-assembly over two decades ago, the use of CNCs to prepare tough Bouligand composites has only received attention in the recent past. Even among these studies, most efforts employ the nanocomposites approach to enhance the flexibility of the iridescent CNC films, rather than the toughness. In the following section, we review the predominant methods for Bouligand CNC composite fabrication (*in situ* polymerization, evaporation-induced self-assembly (EISA)) and evaluate their suitability for successful biomimicry.

4. Fabrication and mechanical properties of Bouligand cellulose nanocrystal composites

(a) *In situ* polymerization

One possible route to preparing PNCs with locked-in 'cholesteric' CNC arrangement is *in situ* polymerization in self-assembled CNC solutions, i.e. through solution coagulation [63]. For instance, MacLachlan *et al.* [64] employed *in situ* polymerization to understand the evolution of liquid crystalline morphology during the self-assembly of CNCs. They prepared suspensions of wood CNCs in aqueous mixtures of polyacrylamide (PAAm) precursors and a photoinitiator. The water was evaporated to reach CNC concentrations beyond the isotropic–biphasic phase boundary for these mixtures. The suspensions were then photopolymerized at concentration steps ranging from 4 to 5% CNC by mass to lock-in the self-assembled tactoids at various stages of their morphological transformation. The authors also prepared near-IR iridescent CNC–PAAm composite hydrogels by employing higher CNC to monomer ratios and photopolymerizing after allowing the solution to evaporate to dryness (62% CNC by mass) [65]. The iridescence in these materials was responsive to solvent, pH and temperature. Tatsumi *et al.* [27] mixed an aqueous solution of 2-hydroxymethyl methacrylate (HEMA) monomer and a radical initiator (hydroxy-2-methylpropiophenone) with wood CNCs at concentrations large enough (5% by mass) to cause separation into isotropic and anisotropic (liquid crystalline) phases. The solutions were later photopolymerized with UV irradiation to lock-in the liquid crystalline structure of the anisotropic phase [27]. However, due to polymerization in solution, these materials lacked dense CNC packing (pitch = 2.8 µm) and had low CNC content (7.1% by mass). Therefore, while these composites exhibited moderate enhancements in modulus over the neat PHEMA polymer, the final material properties were poor in comparison to tough biological composites (figure 4). In a similar vein, Zoppe *et al.* [66] fabricated iridescent films by curing dried films, cast from aqueous mixtures of CNCs, bisphenol diglycidyl ether resin and diamine hardener. The resulting films were calculated to contain 50–72% by mass CNCs. Despite the fairly high CNC content, the resulting moduli were only ≈1 GPa [66].

The *in situ* polymerization technique has the following advantages over EISA. Firstly, the monomeric units enjoy better access to CNC interstitial spaces as compared to the nanometre-scale polymer molecules used in EISA. Further, this technique permits a wider array of polymer matrices (non-polar, non-water-soluble), particularly if the polymerization can be conducted after film casting. Nevertheless, *in situ* polymerization is a complex two-step process. Further, the ability to reliably control polymer concentration and to polymerize at low polymer concentration remains to be demonstrated. Owing to these challenges, this method remains unexplored for the fabrication of tough biomimetic composites.

(b) Templating inorganic composites

MacLachlan and co-workers [74] have demonstrated the use of self-assembled CNCs for templating inorganic materials to produce photonic films of opposite handedness. Here, aqueous suspensions of CNCs in inorganic precursors are allowed to dry and solidify. This way the 'chiral nematic' structure of the self-assembled CNCs can be transferred to inorganic materials

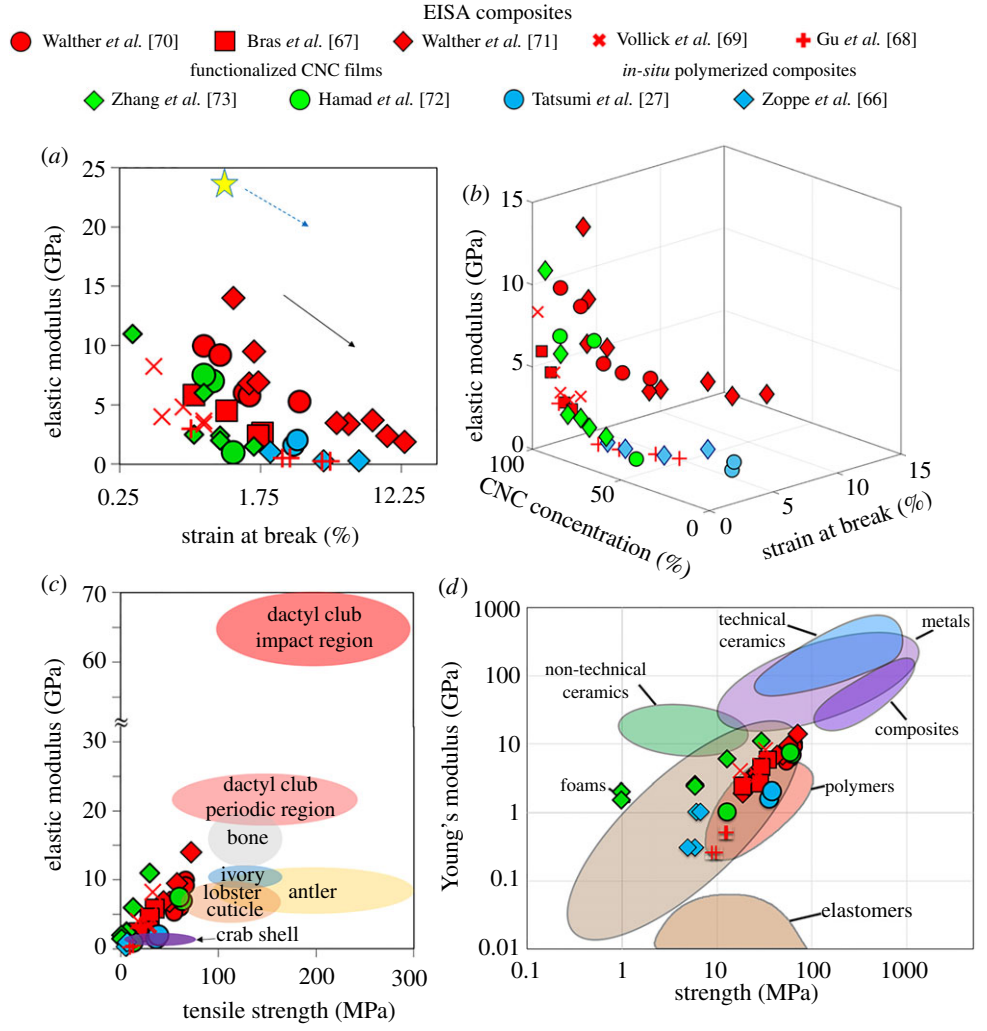

Figure 4. (*a*) Comparative Ashby plot of elastic modulus (GPa) versus the strain at break (%) from Bouligand CNC composites reported in the literature [27,66–73]. The arrow represents the general trend in property change with increased polymer addition. (*b*) A comparative 3D plot of elastic modulus (GPa) versus the strain at break (%) versus the CNC concentration (%) from Bouligand CNC composites reported in the literature. (*c*) An Ashby plot of elastic modulus (GPa) versus the tensile strength (MPa) comparing synthetic Bouligand CNC composites with natural Bouligand materials. (*d*) Ashby plot of elastic modulus (GPa) versus the tensile strength (MPa) comparing synthetic Bouligand CNC composites with commercial materials.

such as TiO_2, metal nitride, (organo)silica using titanium chloride, tetrakis(diethylamido)titanium or tetraethyl orthosilicate precursors, respectively [74]. In these studies, the fabrication of the inorganic–organic composites is typically followed by removal of the CNC phase by calcination, resulting in templated chiral photonic structures. While this technique will probably be useful in future for the mineralization of Bouligand composites, there are currently no reports of the mechanical properties of templated inorganic–organic hybrid CNC materials. Therefore, we do not delve into any further details of the templating technique and refer readers to a detailed review of this technique presented here [74].

(c) Evaporation-induced self-assembly

In this method, CNCs and polymers, mixed in appropriate quantities, are cast into films by slow evaporation of their co-solvent. This is a facile single-step method that offers excellent

control over the amount of polymer, the CNC structure and consequently the film properties. However, the applicability of the technique is limited by the following challenges. Firstly, as-synthesized CNCs are found to have a high negative charge and disperse mainly in water and high-dielectric-constant solvents. This limits the choice of matrices to hydrophilic or water-soluble polymers. Further, because the self-assembly is regulated by the distribution of CNC surface charge, it is preferable for the polymers not to significantly alter the electrostatic CNC–CNC interactions. As an extreme example, Bardet *et al.* [67] observed that sulfated CNCs assembled into 'cholesteric' structures in the presence of anionic (polyacrylate) and neutral (polyethylene glycol) polymers, but formed unstructured aggregates with cationic polyethylenimine. Recent work by Cheung *et al.* [26] has expanded the narrow window of allowable polymers into the non-polar regime. They demonstrated that sulfated CNCs neutralized by positively charged counterions (Na^+, NH_4^+, NMe_4^+), freeze-dried and redispersed in polar organic solvents (dimethyl sulfoxide (DMSO), dimethyl formamide (DMF), formamide), readily form 'cholesteric' phases in the presence of commercial polymers such as polystyrene, poly(methyl methacrylate), polycarbonate and poly(9-vinylcarbazole) [26].

Nevertheless, in line with the above-mentioned limitations, most papers in the literature report the fabrication of Bouligand CNC composites using water-soluble polymers. Bras and co-workers [67] and Gu *et al.* [68] fabricated Bouligand nanocomposites by casting aqueous mixtures of wood CNCs and polyethylene glycol, with qualitatively similar results. With the addition of the polymer, the films displayed enhanced flexibility and an increased strain to failure (figure 4). However, the elastic modulus and tensile strength decreased significantly [67,68]. Vollick *et al.* [69] demonstrated a novel route to enhancing film flexibility through the addition of reactive soft latex nanoparticles. Here, the bottom anisotropic phase, extracted from a biphasic aqueous solution of CNCs with latex nanoparticles and hexamethylenediamine hardener, was cast to obtain flexible photonic films with higher toughness and uncompromised tensile strength. The films, however, were observed to be phase-separated into an isotropic latex-rich top layer and a liquid crystalline CNC-rich bottom layer. Wang & Walther [70] reported a single-step casting process with neutral water-soluble poly(vinyl alcohol) (PVA). The concentration of the PVA was found to control the optical and mechanical properties. The authors reported that the pristine wood CNC films were extremely brittle and could be made more ductile with PVA addition. However, the increased strain to failure was observed to come at the expense of elastic modulus, tensile strength and CNC order (figure 4). Further, they observed that the ordered films broke at small strains (1.5%) due to limited soft-phase dynamics. Zhu *et al*. [71] overcame this problem by casting CNCs with hydrophilic copolymers of poly(oligoethylene glycol methacrylate) and 2-ureido-4-pyrimidinone (UPy) supramolecular units capable of fourfold hydrogen bonding after film formation. The authors demonstrated excellent tunability of mechanical properties by controlling the UPy functional density and CNC concentration, while still maintaining film iridescence [71]. However, similar to their other work, this system suffered from the inverse relationship between ductility and stiffness.

The articles by Walther *et al.* [70,71] revealed another limitation of EISA. The authors observed that the CNC structure transitioned from LC to disordered at polymer fractions greater than 50% by mass [70]. This is not a limitation to making tough composites, as we do not expect high stiffness and strength at these large polymer concentrations. However, they also reported that at polymer concentrations lower than 20% by mass the films were excessively brittle. This is because, at small polymer concentrations, the polymers preferentially fill voids rather than the interstitial space between CNCs. The unfavourable change in entropy of conformation, resulting from polymer stretching to fill interstitial spaces, is probably larger than the favourable entropy of mixing of polymer and CNCs, thereby leading to phase separation. This limitation can be overcome by using cross-linkable low-molecular-weight polymers that favour mixing and suffer lower conformational entropy losses. Alternatively, CNCs may be functionalized with small molecules that act as plasticizers. For example, Vignolini *et al.* [72] demonstrated the fabrication of iridescent CNC films using zwitterionic functionalization, where (dimethyl-myristylammonio)propanesulfonate (DMAPS), a zwitterionic surfactant (and Na^+ counterion)

was absorbed onto CNC through ionic linkages. The micellar structure of the surfactant was hypothesized to act as a spring that enhanced film flexibility [72]. Similarly, Liu *et al.* [73] used 1-allyl-3-methylimidizolium chloride, an ionic liquid, to plasticize iridescent CNCs films, by leaching the ionic liquid through wet, self-assembled CNC membranes. This plasticization effect was attributed to the ability of the ionic liquid to weaken hydrogen bonding between CNCs, thereby promoting the frictional sliding of the particles. In addition to improving the film flexibility, the ionic liquids were also seen to enhance thermal stability and processability [73].

The data from the above-mentioned Bouligand CNC literature are presented as an Ashby plot of Young's modulus versus the strain to failure in figure 4*a*, where the best materials are expected to occupy the top right corner. The following key observations are made from this plot. Firstly, the pristine CNC films are extremely brittle [75] (strain to failure $< 0.5\%$). Indeed, several articles report the inability to measure the properties of the pristine Bouligand films due to their excessively brittle nature [70,72]. Secondly, in all systems, the increased concentration of plasticizers (polymers or small molecules) results in enhanced strain to failure. However, the flexibility enhancement comes at the cost of the tensile modulus and strength [75]. The trends in the mechanical properties with plasticizer addition are highlighted using the black arrow in figure 4*a*. A more detailed plot of the interplay between modulus, strain to failure and CNC concentration is shown in figure 4*b*. The inverse relationship between the stiffness and ductility is the inescapable truth in PNCs. Given this reality, the modulus of the pristine CNC films determines the maximum achievable modulus post-polymer addition. Unfortunately, the moduli of the pristine Bouligand CNC films do not exceed 10–11 GPa, due to which the properties reported in the literature, in large part, are not up to par with the tough biological composites discussed earlier. However, this is an unfair expectation. Most works discussed here were aimed not at biomimicry but rather at improving CNC film flexibility or at enhancing matrix polymer properties. Needless to say, these goals were achieved. But the efforts that do seek to emulate biological composites do so with limited success. An Ashby plot of the modulus versus the tensile strength from the literature data is presented in figure 4*c*. The best of these materials display properties at the lower end of the lobster shell spectrum, but fall well short of the properties of gold standard materials such as bone and the mantis shrimp club.

Further, we note that biological composites are tough without being ductile, owing to their unique microstructure. We note that nacre has as little as 1–5% by mass proteinaceous binder. While this small fraction of binder is probably necessary, the strategy of inelastic toughening through excessive polymer addition is not in line with Nature's approach of extrinsic toughening through structural hierarchy. The Bouligand composites reported in the literature therefore fall squarely in the domain of polymer-like properties as shown in the Ashby plot of commercial materials in figure 4*d*. In order to successfully implement the PNCs strategy to emulate tough biological materials using CNCs, we need the pristine CNC films to be significantly stiffer, stronger and tougher (yellow star in figure 4*a*). This way, even with polymer addition, the final properties will remain comparable to the properties of the best biological materials. The hypothetical trajectory of adding polymer to such a material is highlighted in figure 4*a*. These materials will help fill the desirable but empty top right corner of the mechanical property space.

The CNC building blocks have high modulus and strength ($\approx$150 GPa and $\approx$3 GPa, respectively) [22,23]. However the film properties are dictated by the weakest links and their concentration, i.e. defect sites, voids, CNC–CNC and CNC–polymer interfaces. The uniformity and defect density in CNC films is dictated by dispersity in CNC size and casting kinetics. The CNC size distributions may be narrowed through fractionation or filtration [76]. These monodisperse suspensions cast at lower drying rates are likely to be relatively uniform and defect-free due to reduced glass formation. The uniformity of films may also be enhanced using magnetic and shear fields during film casting [58,77]. The CNC–CNC interfaces may be improved by cross-linking through functionalization or through interface welding by ionic liquids [78] or ion irradiation, as implemented in carbon nanotube films [79]. Shakeri and co-workers [78] have shown toughness enhancements by two orders of magnitude in cellulose microfibre films using nanowelding. The interfaces between CNC and polymer can be compatibilized and strengthened

by a number of means. One option would be to prepare Bouligand films with polymer-grafted CNCs. The grafted chains could be functionalized with cross-linkable groups to enhance stiffness. Alternatively, CNCs functionalized with reactive groups could be employed to promote covalent bonding with polymer matrices through click chemistry after film casting. As discussed earlier, natural composites are stiffened by nanoparticles of minerals such as calcium carbonate and hydroxyapatite. This is achieved through a process known as biomineralization [80]. Here, polymer–mineral nanoparticle complexes are incorporated into ordered fibrils and later directed to form oriented crystal phases. Hard nanoparticles could be incorporated into the self-assembled CNC structure during film casting along with the matrix polymer to achieve similar stiffness enhancements. However, the nanoparticles will have to be on the same size scale or smaller than the CNCs to ensure effective incorporation [81]. The use of mineral precursors as demonstrated by MacLachlan's team might also be applicable for this purpose.

We note that the best enhancements due to Bouligand arrangement in carbon fibre-reinforced composites are seen in impact resistance and bending properties [50]. However, these properties are yet to be measured in CNC Bouligand composites and films. The properties of the minority macromolecular phase in natural composites, which offers binding and energy absorption, are not well characterized. These polymers are probably highly confined in the nanoscale domains between the ordered mineral crystallites. It is well established that the properties of a confined polymer differ significantly from those of the free polymer. However, the effect of polymer confinement on the properties of natural materials is not well understood. The ordered, alternating arrangement of CNCs and polymers in CNC Bouligand composites and the ability to tune the CNC–CNC spacing presents an excellent opportunity to study the properties of natural polymers under confinement. Additionally, the polymers used could be stimuli-responsive, thereby helping to confer environmental sensing capabilities to the Bouligand composites. A key aspect of biological composites thus far not emulated is the network of pore canals that help toughen the material as well as deliver ingredients for self-healing. CNC composites could be cast with or around a network of synthetic nano/micro conduits that help deliver minerals or photopolymerizable monomers to damage sites. These avenues to property enhancement remain open and offer a rich ground for the development of multi-functional CNC-based biomimetic composites.

Data accessibility. This article has no additional data.

Authors' contributions. Both authors contributed equally to the preparation of the manuscript.

Competing interests. We declare we have no competing interests.

Funding. B.N. and J.W.G. acknowledge the support of the Air Force Office of Scientific Research (award no. F1ATA00236G002).

Acknowledgements. We thank Dr Jan Obrzut (NIST) and Dr Caglar Emiroglu (NIST) for useful discussions.

References

1. Egan P, Sinko R, LeDuc PR, Keten S. 2015 The role of mechanics in biological and bio-inspired systems. *Nat. Commun.* **6**, 7418. (doi:10.1038/ncomms8418)
2. Zhang C, McAdams DA, Grunlan JC. 2016 Nano/micro-manufacturing of bioinspired materials: a review of methods to mimic natural structures. *Adv. Mater.* **28**, 6292–6321. (doi:10.1002/adma.201505555)
3. Nikolov S, Petrov M, Lymperakis L, Friák M, Sachs C, Fabritius H-O, Raabe D, Neugebauer J. 2010 Revealing the design principles of high-performance biological composites using ab initio and multiscale simulations: the example of lobster cuticle. *Adv. Mater.* **22**, 519–526. (doi:10.1002/adma.200902019)
4. Wilts BD, Whitney HM, Glover BJ, Steiner U, Vignolini S. 2014 Natural helicoidal structures: morphology, self-assembly and optical properties. *Mater. Today Proc.* **1**, 177–185. (doi:10.1016/j.matpr.2014.09.021)
5. Li X, Chang WC, Chao YJ, Wang R, Chang M. 2004 Nanoscale structural and mechanical characterization of a natural nanocomposite material: the shell of red abalone. *Nano Lett.* **4**, 613–617. (doi:10.1021/nl049962k)

6. Neville AC. 1986 The physics of helicoids. *Phys. Bull.* **37**, 74–76. (doi:10.1088/0031-9112/37/2/028)
7. Weaver JC *et al.* 2012 The stomatopod dactyl club: a formidable damage-tolerant biological hammer. *Science* **336**, 1275–1280. (doi:10.1126/science.1218764)
8. Barth HD, Zimmermann EA, Schaible E, Tang SY, Alliston T, Ritchie RO. 2011 Characterization of the effects of x-ray irradiation on the hierarchical structure and mechanical properties of human cortical bone. *Biomaterials* **32**, 8892–8904. (doi:10.1016/j.biomaterials.2011.08.013)
9. Yaraghi NA *et al.* 2016 A sinusoidally architected helicoidal biocomposite. *Adv. Mater.* **28**, 6835–6844. (doi:10.1002/adma.201600786)
10. Bouligand Y. 1972 Twisted fibrous arrangements in biological materials and cholesteric mesophases. *Tissue Cell* **4**, 189–217. (doi:10.1016/S0040-8166(72)80042-9)
11. Raabe D, Sachs C, Romano P. 2005 The crustacean exoskeleton as an example of a structurally and mechanically graded biological nanocomposite material. *Acta Mater.* **53**, 4281–4292. (doi:10.1016/j.actamat.2005.05.027)
12. Locke M. 2008 Structure of ivory. *J. Morphol.* **269**, 423–450. (doi:10.1002/jmor.10585)
13. Rho JY, Kuhn-Spearing L, Zioupos P. 1998 Mechanical properties and the hierarchical structure of bone. *Med. Eng. Phys.* **20**, 92–102. (doi:10.1016/S1350-4533(98)00007-1)
14. Launey ME, Buehler MJ, Ritchie RO. 2010 On the mechanistic origins of toughness in bone. *Annu. Rev. Mater. Res.* **40**, 25–53. (doi:10.1146/annurev-matsci-070909-104427)
15. Meyers MA, Chen P-Y, Lin AY-M, Seki Y. 2008 Biological materials: structure and mechanical properties. *Prog. Mater. Sci.* **53**, 1–206. (doi:10.1016/j.pmatsci.2007.05.002)
16. Yang Y, Chen Z, Song X, Zhang Z, Zhang J, Shung KK, Zhou Q, Chen Y. 2017 Biomimetic anisotropic reinforcement architectures by electrically assisted nanocomposite 3D printing. *Adv. Mater.* **29**, 1605750. (doi:10.1002/adma.201605750)
17. Lagerwall JPF, Schütz C, Salajkova M, Noh J, Park JH, Scalia G, Bergström L. 2014 Cellulose nanocrystal-based materials: from liquid crystal self-assembly and glass formation to multifunctional thin films. *NPG Asia Mater.* **6**, e80. (doi:10.1038/am.2013.69)
18. Moon RJ, Martini A, Nairn J, Simonsen J, Youngblood J. 2011 Cellulose nanomaterials review: structure, properties and nanocomposites. *Chem. Soc. Rev.* **40**, 3941. (doi:10.1039/c0cs00108b)
19. Sacui IA, Nieuwendaal RC, Burnett DJ, Stranick SJ, Jorfi M, Weder C, Foster EJ, Olsson RT, Gilman JW. 2014 Comparison of the properties of cellulose nanocrystals and cellulose nanofibrils isolated from bacteria, tunicate, and wood processed using acid, enzymatic, mechanical, and oxidative methods. *ACS Appl. Mater. Interfaces* **6**, 6127–6138. (doi:10.1021/am500359f)
20. Sapkota J, Shirole A, Foster EJ, Martinez Garcia JC, Lattuada M, Weder C. 2017 Polymer nanocomposites with nanorods having different length distributions. *Polymer* **110**, 284–291. (doi:10.1016/j.polymer.2016.12.010)
21. Habibi Y, Lucia LA, Rojas OJ. 2010 Cellulose nanocrystals: chemistry, self-assembly, and applications. *Chem. Rev.* **110**, 3479–3500. (doi:10.1021/cr900339w)
22. Šturcová A, Davies GR, Eichhorn SJ. 2005 Elastic modulus and stress-transfer properties of tunicate cellulose whiskers. *Biomacromolecules* **6**, 1055–1061. (doi:10.1021/bm049291k)
23. Saito T, Kuramae R, Wohlert J, Berglund LA, Isogai A. 2013 An ultrastrong nanofibrillar biomaterial: the strength of single cellulose nanofibrils revealed via sonication-induced fragmentation. *Biomacromolecules* **14**, 248–253. (doi:10.1021/bm301674e)
24. Mehr SHM, Giese M, Qi H, Shopsowitz KE, Hamad WY, MacLachlan MJ. 2013 Novel PPV/mesoporous organosilica composites: influence of the host chirality on a conjugated polymer guest. *Langmuir* **29**, 12 579–12 584. (doi:10.1021/la4024597)
25. Giese M, Khan MK, Hamad WY, MacLachlan MJ. 2013 Imprinting of photonic patterns with thermosetting amino–formaldehyde–cellulose composites. *ACS Macro Lett.* **2**, 818–821. (doi:10.1021/mz4003722)
26. Cheung CCY, Giese M, Kelly JA, Hamad WY, MacLachlan MJ. 2013 Iridescent chiral nematic cellulose nanocrystal/polymer composites assembled in organic solvents. *ACS Macro Lett.* **2**, 1016–1020. (doi:10.1021/mz400464d)
27. Tatsumi M, Teramoto Y, Nishio Y. 2012 Polymer composites reinforced by locking-in a liquid-crystalline assembly of cellulose nanocrystallites. *Biomacromolecules* **13**, 1584–1591. (doi:10.1021/bm300310f)

28. Grunenfelder LK, Herrera S, Kisailus D. 2014 Crustacean-derived biomimetic components and nanostructured composites. *Small* **10**, 3207–3232. (doi:10.1002/smll.201400559)
29. Guarín-Zapata N, Gomez J, Yaraghi N, Kisailus D, Zavattieri PD. 2015 Shear wave filtering in naturally-occurring Bouligand structures. *Acta Biomater.* **23**, 11–20. (doi:10.1016/j.actbio.2015.04.039)
30. Zimmermann EA, Gludovatz B, Schaible E, Dave NKN, Yang W, Meyers MA, Ritchie RO. 2013 Mechanical adaptability of the Bouligand-type structure in natural dermal armour. *Nat. Commun.* **4**, 2634. (doi:10.1038/ncomms3634)
31. Raabe D, Romano P, Sachs C, Al-Sawalmih A, Brokmeier H-G, Yi S-B, Servos G, Hartwig HG. 2005 Discovery of a honeycomb structure in the twisted plywood patterns of fibrous biological nanocomposite tissue. *J. Cryst. Growth* **283**, 1–7. (doi:10.1016/j.jcrysgro.2005.05.077)
32. Charvolin J, Sadoc J-F. 2012 About collagen, a tribute to Yves Bouligand. *Interface Focus* **2**, 567–574. (doi:10.1098/rsfs.2012.0014)
33. Bouligand Y, Giraud-Guille M-M. 1985 Spatial organization of collagen fibrils in skeletal tissues: analogies with liquid crystals. In *Biology of invertebrate and lower vertebrate collagens*, pp. 115–134. Boston, MA: Springer.
34. Bouligand Y. 1986 Theory of microtomy artefacts in arthropod cuticle. *Tissue Cell* **18**, 621–643. (doi:10.1016/0040-8166(86)90025-X)
35. Bouligand Y. 2008 Liquid crystals and biological morphogenesis: ancient and new questions. *Comptes Rendus Chim.* **11**, 281–296. (doi:10.1016/j.crci.2007.10.001)
36. Giraud MM, Castanet J, Meunier FJ, Bouligand Y. 1978 The fibrous structure of coelacanth scales: a twisted 'plywood'. *Tissue Cell* **10**, 671–686. (doi:10.1016/0040-8166(78)90054-X)
37. Chen PY, Lin AYM, McKittrick J, Meyers MA. 2008 Structure and mechanical properties of crab exoskeletons. *Acta Biomater.* **4**, 587–596. (doi:10.1016/j.actbio.2007.12.010)
38. Chen PY, Lin AYM, Lin YS, Seki Y, Stokes AG, Peyras J, Olevsky E, Meyers M, McKittrick J. 2008 Structure and mechanical properties of selected biological materials. *J. Mech. Behav. Biomed. Mater.* **1**, 208–226. (doi:10.1016/j.jmbbm.2008.02.003)
39. Sachs C, Fabritius H, Raabe D. 2008 Influence of microstructure on deformation anisotropy of mineralized cuticle from the lobster *Homarus americanus*. *J. Struct. Biol.* **161**, 120–132. (doi:10.1016/j.jsb.2007.09.022)
40. Blob RW, Snelgrove JM. 2006 Antler stiffness in moose (*Alces alces*): correlated evolution of bone function and material properties? *J. Morphol.* **267**, 1075–1086. (doi:10.1002/jmor.10461)
41. Jakubinek MB, Samarasekera CJ, White MA. 2006 Elephant ivory: a low thermal conductivity, high strength nanocomposite. *J. Mater. Res.* **21**, 287–292. (doi:10.1557/jmr.2006.0029)
42. Nweeia MT *et al.* 2014 Sensory ability in the narwhal tooth organ system. *Anat. Rec.* **297**, 599–617. (doi:10.1002/ar.22886)
43. Yang W *et al.* 2014 Protective role of *Arapaima gigas* fish scales: structure and mechanical behavior. *Acta Biomater.* **10**, 3599–3614. (doi:10.1016/j.actbio.2014.04.009)
44. Lin YS, Wei CT, Olevsky EA, Meyers MA. 2011 Mechanical properties and the laminate structure of *Arapaima gigas* scales. *J. Mech. Behav. Biomed. Mater.* **4**, 1145–1156. (doi:10.1016/j.jmbbm.2011.03.024)
45. Yang R, Zaheri A, Gao W, Hayashi C, Espinosa HD. 2017 AFM identification of beetle exocuticle: Bouligand structure and nanofiber anisotropic elastic properties. *Adv. Funct. Mater.* **27**, 1603993. (doi:10.1002/adfm.201603993)
46. Vignolini S *et al.* 2012 Pointillist structural color in *Pollia* fruit. *Proc. Natl Acad. Sci. USA* **109**, 15 715. (doi:10.1073/pnas.1210105109)
47. Gubb D. 1975 A direct visualisation of helicoidal architecture in *Carcinus maenas* and *Halocynthia papillosa* by scanning electron microscopy. *Tissue Cell* **7**, 19–32. (doi:10.1016/S0040-8166)
48. Cheng L, Thomas A, Glancey JL, Karlsson AM. 2011 Mechanical behavior of bio-inspired laminated composites. *Compos. A: Appl. Sci. Manuf.* **42**, 211–220. (doi:10.1016/j.compositesa.2010.11.009)
49. Chen B, Peng X, Cai C, Niu H, Wu X. 2006 Helicoidal microstructure of Scarabaei cuticle and biomimetic research. *Mater. Sci. Eng. A* **423**, 237–242. (doi:10.1016/j.msea.2005.11.069)
50. Grunenfelder LK *et al.* 2014 Bio-inspired impact-resistant composites. *Acta Biomater.* **10**, 3997–4008. (doi:10.1016/j.actbio.2014.03.022)
51. Apichattrabrut T, Ravi-Chandar K. 2006 Helicoidal composites. *Mech. Adv. Mater. Struct.* **13**, 61–76. (doi:10.1080/15376490500343808)

52. Revol JF, Bradford H, Giasson J, Marchessault RH, Gray DG. 1992 Helicoidal self-ordering of cellulose microfibrils in aqueous suspension. *Int. J. Biol. Macromol.* **14**, 170–172. (doi:10.1016/S0141-8130(05)80008-X)
53. Zhang YP, Chodavarapu VP, Kirk AG, Andrews MP. 2012 Nanocrystalline cellulose for covert optical encryption. *J. Nanophotonics* **6**, 63 516–63 519. (doi:10.1117/1.JNP.6.063516)
54. Zhao Z, Shklyaev OE, Nili A, Mohamed MNA, Kubicki JD, Crespi VH, Zhong L. 2013 Cellulose microfibril twist, mechanics, and implication for cellulose biosynthesis. *J. Phys. Chem. A* **117**, 2580–2589. (doi:10.1021/jp3089929)
55. Paavilainen S, Róg T, Vattulainen I. 2011 Analysis of twisting of cellulose nanofibrils in atomistic molecular dynamics simulations. *J. Phys. Chem. B* **115**, 3747–3755. (doi:10.1021/jp111459b)
56. Usov I, Nyström G, Adamcik J, Handschin S, Schütz C, Fall A, Bergström L, Mezzenga R. 2015 Understanding nanocellulose chirality and structure–properties relationship at the single fibril level. *Nat. Commun.* **6**, 7564. (doi:10.1038/ncomms8564)
57. Natarajan B, Emiroglu C, Obrzut J, Fox DM, Pazmino B, Douglas JF, Pazmino B, Douglas JF, Gilman JW. 2017 Dielectric characterization of confined water in chiral cellulose nanocrystal films. *ACS Appl. Mater. Interfaces* **9**, 14 222–14 231. (doi:10.1021/acsami.7b01674)
58. Pan J, Hamad W, Straus SK. 2010 Parameters affecting the chiral nematic phase of nanocrystalline cellulose films. *Macromolecules* **43**, 3851–3858. (doi:10.1021/ma902383k)
59. Beck S, Bouchard J, Chauve G, Berry R. 2013 Controlled production of patterns in iridescent solid films of cellulose nanocrystals. *Cellulose* **20**, 1401–1411. (doi:10.1007/s10570-013-9888-4)
60. Dumanli AG, Kamita G, Landman J, van der Kooij H, Glover BJ, Baumberg JJ, Steiner U, Vignolini S. 2014 Controlled, bio-inspired self-assembly of cellulose-based chiral reflectors. *Adv. Opt. Mater.* **2**, 646–650. (doi:10.1002/adom.201400112)
61. Frka-Petesic B, Radavidson H, Jean B, Heux L. 2017 Dynamically controlled iridescence of cholesteric cellulose nanocrystal suspensions using electric fields. *Adv. Mater.* **29**, 1606208. (doi:10.1002/adma.201606208)
62. Fernandes SN, Almeida PL, Monge N, Aguirre LE, Reis D, de Oliveira CLP, Neto AMF, Pieranski P, Godinho MH. 2017 Mind the microgap in iridescent cellulose nanocrystal films. *Adv. Mater.* **29**, 1603560. (doi:10.1002/adma.201603560)
63. Khan MK, Giese M, Yu M, Kelly JA, Hamad WY, MacLachlan MJ. 2013 Flexible mesoporous photonic resins with tunable chiral nematic structures. *Angew. Chem. Int. Ed.* **52**, 8921–8924. (doi:10.1002/anie.201303829)
64. Wang P-X, Hamad WY, MacLachlan MJ. 2016 Structure and transformation of tactoids in cellulose nanocrystal suspensions. *Nat. Commun.* **7**, 11515. (doi:10.1038/ncomms11515)
65. Kelly JA, Shukaliak AM, Cheung CCY, Shopsowitz KE, Hamad WY, MacLachlan MJ. 2013 Responsive photonic hydrogels based on nanocrystalline cellulose. *Angew. Chem. Int. Ed.* **52**, 8912–8916. (doi:10.1002/anie.201302687)
66. Zoppe JO, Grosset L, Seppälä J. 2013 Liquid crystalline thermosets based on anisotropic phases of cellulose nanocrystals. *Cellulose* **20**, 2569–2582. (doi:10.1007/s10570-013-0008-2)
67. Bardet R, Belgacem N, Bras J. 2015 Flexibility and color monitoring of cellulose nanocrystal iridescent solid films using anionic or neutral polymers. *ACS Appl. Mater. Interfaces* **7**, 4010–4018. (doi:10.1021/am506786t)
68. Gu M, Jiang C, Liu D, Prempeh N, Smalyukh II. 2016 Cellulose nanocrystal/poly(ethylene glycol) composite as an iridescent coating on polymer substrates: structure–color and interface adhesion. *ACS Appl. Mater. Interfaces* **8**, 32 565–32 573. (doi:10.1021/acsami.6b12044)
69. Vollick B, Kuo P-Y, Thérien-Aubin H, Yan N, Kumacheva E. 2017 Composite cholesteric nanocellulose films with enhanced mechanical properties. *Chem. Mater.* **29**, 789–795. (doi:10.1021/acs.chemmater.6b04780)
70. Wang B, Walther A. 2015 Self-assembled, iridescent, crustacean-mimetic nanocomposites with tailored periodicity and layered cuticular structure. *ACS Nano* **9**, 10 637–10 646. (doi:10.1021/acsnano.5b05074)
71. Zhu B, Merindol R, Benitez AJ, Wang B, Walther A. 2016 Supramolecular engineering of hierarchically self-assembled, bioinspired, cholesteric nanocomposites formed by cellulose nanocrystals and polymers. *ACS Appl. Mater. Interfaces* **8**, 11 031–11 040. (doi:10.1021/acsami.6b00410)
72. Guidetti G, Atifi S, Vignolini S, Hamad WY. 2016 Flexible photonic cellulose nanocrystal films. *Adv. Mater.* **28**, 10 042–10 047. (doi:10.1002/adma.201603386)

73. Liu P, Guo X, Nan F, Duan Y, Zhang J. 2017 Modifying mechanical, optical properties and thermal processability of iridescent cellulose nanocrystal films using ionic liquid. *ACS Appl. Mater. Interfaces* **9**, 3085–3092. (doi:10.1021/acsami.6b12953)
74. Giese M, Blusch LK, Khan MK, MacLachlan MJ. 2015 Functional materials from cellulose-derived liquid-crystal templates. *Angew. Chem. Int. Ed.* **54**, 2888–2910. (doi:10.1002/anie.201407141)
75. Passantino JM, Haywood AD, Goswami J, Davis VA. 2017 Effects of polymer additives and dispersion state on the mechanical properties of cellulose nanocrystal films. *Macromol. Mater. Eng.* **302**, 1600351. (doi:10.1002/mame.201600351)
76. Hu Y, Abidi N. 2016 Distinct chiral nematic self-assembling behavior caused by different size-unified cellulose nanocrystals via a multistage separation. *Langmuir* **32**, 9863–9872. (doi:10.1021/acs.langmuir.6b02861)
77. Park JH, Noh J, Schütz C, Salazar-Alvarez G, Scalia G, Bergström L, Lagerwall JPF. 2014 Macroscopic control of helix orientation in films dried from cholesteric liquid-crystalline cellulose nanocrystal suspensions. *ChemPhysChem* **15**, 1477–1484. (doi:10.1002/cphc.201400062)
78. Yousefi H, Nishino T, Faezipour M, Ebrahimi G, Shakeri A. 2011 Direct fabrication of all-cellulose nanocomposite from cellulose microfibers using ionic liquid-based nanowelding. *Biomacromolecules* **12**, 4080–4085. (doi:10.1021/bm201147a)
79. Williams TS *et al.* 2016 Trade-off between the mechanical strength and microwave electrical properties of functionalized and irradiated carbon nanotube sheets. *ACS Appl. Mater. Interfaces* **8**, 9327–9334. (doi:10.1021/acsami.5b12303)
80. Colfen H. 2010 Biomineralization: a crystal-clear view. *Nat. Mater.* **9**, 960–961. (doi:10.1038/nmat2911)
81. Schlesinger M, Giese M, Blusch LK, Hamad WY, MacLachlan MJ. 2015 Chiral nematic cellulose–gold nanoparticle composites from mesoporous photonic cellulose. *Chem. Commun.* **51**, 530–533. (doi:10.1039/C4CC07596J)